

## Thin Shell, High Velocity Inertial Confinement Fusion Implosions on the National Ignition Facility

T. Ma,<sup>1</sup> O. A. Hurricane,<sup>1</sup> D. A. Callahan,<sup>1</sup> M. A. Barrios,<sup>1</sup> D. T. Casey,<sup>1</sup> E. L. Dewald,<sup>1</sup> T. R. Dittrich,<sup>1</sup> T. Döppner,<sup>1</sup> S. W. Haan,<sup>1</sup> D. E. Hinkel,<sup>1</sup> L. F. Berzak Hopkins,<sup>1</sup> S. Le Pape,<sup>1</sup> A. G. MacPhee,<sup>1</sup> A. Pak,<sup>1</sup> H.-S. Park,<sup>1</sup> P. K. Patel,<sup>1</sup> B. A. Remington,<sup>1</sup> H. F. Robey,<sup>1</sup> J. D. Salmonson,<sup>1</sup> P. T. Springer,<sup>1</sup> R. Tommasini,<sup>1</sup> L. R. Benedetti,<sup>1</sup> R. Bionta,<sup>1</sup> E. Bond,<sup>1</sup> D. K. Bradley,<sup>1</sup> J. Caggiano,<sup>1</sup> P. Celliers,<sup>1</sup> C. J. Cerjan,<sup>1</sup> J. A. Church,<sup>1</sup> S. Dixit,<sup>1</sup> R. Dylla-Spears,<sup>1</sup> D. Edgell,<sup>2</sup> M. J. Edwards,<sup>1</sup> J. Field,<sup>1</sup> D. N. Fittinghoff,<sup>1</sup> J. A. Frenje,<sup>3</sup> M. Gatu Johnson,<sup>3</sup> G. Grim,<sup>4</sup> N. Guler,<sup>4</sup> R. Hatarik,<sup>1</sup> H. W. Herrmann,<sup>4</sup> W. W. Hsing,<sup>1</sup> N. Izumi,<sup>1</sup> O. S. Jones,<sup>1</sup> S. F. Khan,<sup>1</sup> J. D. Kilkenny,<sup>5</sup> J. Knauer,<sup>2</sup> T. Kohut,<sup>1</sup> B. Koziowski,<sup>1</sup> A. Kritcher,<sup>1</sup> G. Kyrala,<sup>4</sup> O. L. Landen,<sup>1</sup> B. J. MacGowan,<sup>1</sup> A. J. Mackinnon,<sup>1</sup> N. B. Meezan,<sup>1</sup> F. E. Merrill,<sup>4</sup> J. D. Moody,<sup>1</sup> S. R. Nagel,<sup>1</sup> A. Nikroo,<sup>5</sup> T. Parham,<sup>1</sup> J. E. Ralph,<sup>1</sup> M. D. Rosen,<sup>1</sup> J. R. Rygg,<sup>1</sup> J. Sater,<sup>1</sup> D. Sayre,<sup>1</sup> M. B. Schneider,<sup>1</sup> D. Shaughnessy,<sup>1</sup> B. K. Spears,<sup>1</sup> R. P. J. Town,<sup>1</sup> P. L. Volegov,<sup>4</sup> A. Wan,<sup>1</sup> K. Widmann,<sup>1</sup> C. H. Wilde,<sup>4</sup> and C. Yeamans<sup>1</sup>

<sup>1</sup>Lawrence Livermore National Laboratory, Livermore, California 94550, USA

<sup>2</sup>Laboratory for Laser Energetics, University of Rochester, Rochester, New York 14623, USA

<sup>3</sup>Massachusetts Institute of Technology Plasma Science and Fusion Center, Cambridge, Massachusetts 02139, USA

<sup>4</sup>Los Alamos National Laboratory, Los Alamos, New Mexico 87545, USA

<sup>5</sup>General Atomics, San Diego, California 92186, USA

(Received 15 December 2014; published 6 April 2015)

Experiments have recently been conducted at the National Ignition Facility utilizing inertial confinement fusion capsule ablators that are 175 and 165  $\mu\text{m}$  in thickness, 10% and 15% thinner, respectively, than the nominal thickness capsule used throughout the high foot and most of the National Ignition Campaign. These three-shock, high-adiabat, high-foot implosions have demonstrated good performance, with higher velocity and better symmetry control at lower laser powers and energies than their nominal thickness ablator counterparts. Little to no hydrodynamic mix into the DT hot spot has been observed despite the higher velocities and reduced depth for possible instability feedthrough. Early results have shown good repeatability, with up to 1/2 the neutron yield coming from  $\alpha$ -particle self-heating.

DOI: 10.1103/PhysRevLett.114.145004

PACS numbers: 52.57.Fg

In the quest to achieve ignition through the inertial confinement fusion scheme [1], one of the critical challenges is to drive a symmetric implosion at high velocities without hydrodynamic instabilities becoming detrimental. At the National Ignition Facility (NIF) [2,3], the indirect-drive approach is being pursued, where laser energy is incident on the inner wall of a high- $Z$  hohlraum to generate a high flux of soft x rays which then ablatively drives the implosion of a spherical capsule. In a rocketlike momentum conservation reaction, as the ablator material absorbs the x rays and explodes outward, the shell and fuel layer are accelerated inward. In order to achieve thermonuclear burn, the fuel must reach a peak velocity of  $V_{\text{fuel}} \geq 350$  km/s in order to assemble a hot spot of sufficient temperature ( $> 4$  keV) with a hot spot areal density of  $\rho R > 0.3$  g/cm<sup>2</sup> and DT fuel with  $\rho R > 1$  g/cm<sup>2</sup> [4].

An efficient acceleration of the shell is a tradeoff between minimum remaining unablated mass (i.e., ablation pressure can do its work on the least amount of payload mass) while protecting the fuel and hot spot from feedthrough of instabilities that grow at the ablation front and penetrate in. Because shell velocity scales with laser

energy, and inversely with ablator mass, ablator thickness can be traded for laser energy. Here we report on experiments building on the high-adiabat, high-foot implosions described in Refs. [5–7], but now using 10% and 15% thinner ablators to achieve similar velocities with less laser energy and power. These experiments have demonstrated improved shape control, good repeatability, and performance scaling with laser power and energy. Crucially, little to no mix of ablator material into the hot spot has been observed, despite the higher velocities. These thinner ablator implosions have also shown significant  $\alpha$ -particle deposition leading to considerable self-heating.

Previous work during the National Ignition Campaign (NIC) had shown that instabilities seeded at the ablation front were a significant source of mix into the hot spot on the highest velocity NIC shots [8]. Backlit measurements of the shell as it converged [9] showed a lower-than-expected ablator mass at a given velocity [10]. Larger shell thicknesses were chosen and tested to increase the remaining mass and thus reduce instability feedthrough. These implosions, driven with the NIC four-shock low-foot pulse shape at 420 TW, 1.9 MJ, continued to show unacceptable levels of mix despite the thicker ablator. The more recent

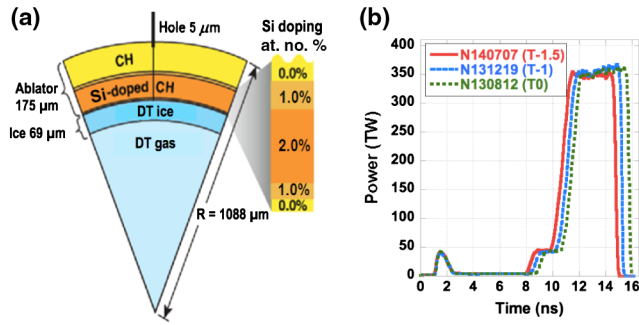


FIG. 1 (color online). (a) Schematic of  $T$ -1 capsule showing dimensions. The undoped CH layer on the outside is an additional  $10\ \mu\text{m}$  thinner in the  $T$ -1.5 capsule. (b) Laser pulse shapes used to drive the  $T$ -1.5 ablator implosion  $N140707$ , the  $T$ -1  $N131219$ , and the counterpart  $T0$   $N130812$ .

results we present here use the high-foot drive, giving higher initial radiation temperature in the “foot” of the pulse, placing the implosion on a higher DT fuel adiabat ( $\sim 2$ – $2.5$ ) and thereby increasing both ablation rates and density gradient scale lengths of the shell [11,12]. Using this pulse shape, targets identical to the nominal NIC Rev. 5 capsule [13] (which employed an ablator of  $195\ \mu\text{m}$  thickness, so-called  $T0$ ) were stable, with low levels of mix, even when driven at laser energies of  $1.9\ \text{MJ}$  and peak powers exceeding  $420\ \text{TW}$ . The in-flight aspect ratio (IFAR) is defined as the ratio between the inner radius of the ablator and the ablator thickness and is a metric of the susceptibility of the shell to instability feedthrough. As the IFAR of the high-foot implosion is predicted to be substantially lower than the low-foot IFAR throughout the majority of the implosion [14], there was latitude to test the thinner ablators to increase velocity.

Figure 1 shows a capsule pie diagram of the cryogenically layered capsule with the 10% thinner ablator. An outer shell of CH plastic surrounds concentric layers with varying levels of Si dopant. The total thickness of the shell shown is  $175\ \mu\text{m}$  (called  $T$ -1 shell), a decrease of  $20\ \mu\text{m}$  from previous high-foot implosions, all of which used the  $195\ \mu\text{m}$  thick ( $T0$ ) ablator. The reduction in ablator thickness is taken from the outer undoped layer, while holding the inner ablator radius constant (i.e., outer radius is now  $1110\ \mu\text{m}$  rather than the nominal  $1130\ \mu\text{m}$ ). In the case of the 15% thinner ablator, the total thickness of the shell is  $165\ \mu\text{m}$  ( $T$ -1.5 shell), with outer radius of  $1100\ \mu\text{m}$ . The ablator then encloses a spherical shell of cryogenic 50:50 DT ice of  $69\ \mu\text{m}$ , which in turn surrounds a central sphere of DT vapor in equilibrium with the solid DT. The Au hohlraum dimensions are  $5.75\ \text{mm}$  in diameter,  $9.43\ \text{mm}$  long, with  $3.1\ \text{mm}$  diameter laser-entrance holes. The hohlraums are filled with  $1.6\ \text{mg}/\text{cm}^3$  of  $^4\text{He}$  gas to restrict the plasma expansion of the hohlraum wall. These targets were shot at a temperature of  $18.6\ \text{K}$ .

The laser pulse used to drive a set of comparison shots testing the  $T0$ ,  $T$ -1, and  $T$ -1.5 capsules at  $350\ \text{TW}$  are

shown. As can be seen, the second and third rises are brought in earlier for the thinner ablators, as the time required for the shocks to propagate across the width of the ablator is decreased. Thus, the shortening of the laser pulse also reduces the overall laser energy required to drive the implosion. The peak powers and energies for the three  $T$ -1 and one  $T$ -1.5 capsule shots discussed in this Letter ranged from  $345$  to  $393\ \text{TW}$ , and  $1.57$  to  $1.75\ \text{MJ}$ .

Implosions where the center of mass of the remaining ablator material was radiographically backlit [15] were used to measure the in-flight shape, mass remaining, and velocity of the various thickness shell implosions. These “2DConA’s” showed that as the ablator thickness was reduced, the three-color wavelength separation, or  $\Delta\lambda$ , required to maintain in-flight and hot-spot symmetry was correspondingly lowered [14]. Changing the wavelength of the separate cones of laser beams allows for controlling the energy transfer between the beams when they cross, and can be advantageously used to adjust the symmetry of the implosion [16]. The  $T$ -1 and  $T$ -1.5 shells at  $200\ \mu\text{m}$  radius, as well as the hot spot at stagnation, were seen to be more elongated along the hohlraum axis, indicating improved inner beam propagation into the hohlraum (and therefore increased drive at the hohlraum waist) as compared to the  $T0$  capsules at comparable or lower  $\Delta\lambda$ . This is attributed to two hohlraum benefits afforded by the thinner ablator: (1) less potential ablator mass filling the hohlraum and (2) distribution of the ablator mass at smaller radius as compared to a thicker ablator since the thinner ablator implosions accelerate inwards sooner during the early epochs of the laser pulse. The shorter laser pulse may also change the amount of hohlraum material blowoff and the distance it is able to travel.

Cryogenically layered DT implosions were subsequently fielded. The measured and inferred implosion performance metrics for four thin shell implosions and two comparison nominal ablator shots are tabulated in Table I. The DT neutron yields are measured with the neutron time of flight [17], foil activation [18], and magnetic recoil spectrometer [19] diagnostics, and the reported values represent weighted averages between those independent measurements.

Hot spot ion temperatures ( $T_{\text{ion}}$ ), determined from the Doppler broadening of the DT peak, remain high for all the thinner ablator shots, indicating low conductive and radiative losses due to mix, consistent with the yield performance and level of  $\alpha$  heating.

Also measured by the nuclear diagnostics is the down-scattered ratio (DSR), which is proportional to the areal density  $\rho R$  of the fuel surrounding the neutron producing plasma [21,22]. It is notable that the DSR of  $4.11 \pm 0.22\%$  ( $\sim \rho R_{\text{fuel}}$  of  $0.91\ \text{g}/\text{cm}^2$ ) achieved with the  $T$ -1.5 ablator used on  $N140707$  is actually the highest DSR recorded for any of the implosions driven with a high-foot pulse shape, including  $T0$  and  $T$ -1 capsules, indicating that a  $165\ \mu\text{m}$

TABLE I. Summary of experimentally measured and inferred\* performance parameters [20] from the thin shell high-foot implosion shots, and selected  $T0$  shots for comparison.

	Comparison shots at 350 TW			Identical yields		Repeat of $N131219$
	$N130812$	$N131219$	$N140707$	$N131119$	$N140311$	$N140225$
Capsule thickness	$T0: 195.5 \mu\text{m}$	$T-1: 173.2 \mu\text{m}$	$T-1.5: 163.7 \mu\text{m}$	$T0: 193.9 \mu\text{m}$	$T-1: 177.2 \mu\text{m}$	$T-1: 177.2 \mu\text{m}$
Laser energy (MJ)	1.69	1.62	1.57	1.91	1.75	1.57
Peak power (TW)	354.9	357.1	348.1	427.5	392.5	345.3
$\Delta\lambda: \lambda_{30}/\lambda_{23}$ (Å)	7.3/8.5	6.2/6.9	5.2/5.9	8.8/9.5	6.2/6.9	6.2/6.9
DT yield (13–15 MeV)	$2.4 \pm 0.1 \times 10^{15}$	$3.0 \pm 0.06 \times 10^{15}$	$4.2 \pm 0.12 \times 10^{15}$	$5.2 \pm 0.1 \times 10^{15}$	$5.2 \pm 0.09 \times 10^{15}$	$2.8 \pm 0.05 \times 10^{15}$
$T_{\text{ion}}$ (DT) (keV)	$4.02 \pm 0.16$	$4.91 \pm 0.15$	$4.65 \pm 0.12$	$4.83 \pm 0.15$	$5.36 \pm 0.15$	$4.51 \pm 0.15$
DSR (%)	$3.96 \pm 0.16$	$3.80 \pm 0.30$	$4.11 \pm 0.23$	$3.40 \pm 0.27$	$3.97 \pm 0.23$	$3.70 \pm 0.20$
X-ray bang time (ns)	$16.74 \pm 0.02$	$16.03 \pm 0.02$	$15.35 \pm 0.02$	$16.40 \pm 0.02$	$16.14 \pm 0.02$	$16.28 \pm 0.02$
X-ray burn (ps)	$162 \pm 3$	$147 \pm 2$	$121 \pm 6$	$152 \pm 33$	$115 \pm 29$	$113 \pm 28$
$P_0$ ( $\mu\text{m}$ ) (x ray)	$35.78 \pm 2.73$	$30.8 \pm 1.48$	$29.08 \pm 1.35$	$37.52 \pm 1.39$	$33.82 \pm 1.03$	$30.84 \pm 1.48$
$P_2$ ( $\mu\text{m}$ ) (x ray)	$-7.66 \pm 3.69$	$-1.37 \pm 1.18$	$-5.77 \pm 0.63$	$-10.63 \pm 1.42$	$-8.52 \pm 0.81$	$-2.61 \pm 0.76$
$M_0$ ( $\mu\text{m}$ ) (x ray)	$44.56 \pm 1.52$	$34.63 \pm 1.13$	$35.10 \pm 1.77$	$51.68 \pm 4.06$	$44.71 \pm 1.95$	$34.83 \pm 1.37$
$P_0$ ( $\mu\text{m}$ ) (neutron)	$35.16 \pm 4.0$	$33.13 \pm 4.0$	$27.34 \pm 4.0$	$37.23 \pm 4.0$	$33.07 \pm 4.0$	$28.95 \pm 4.0$
Fuel velocity (km/s)*	$325 \pm 20$	$348 \pm 30$	$350 \pm 30$	$352 \pm 30$	$372 \pm 30$	$334 \pm 30$
Mix mass (ng)*	$0 \pm 160$	$45 \pm 92$	$0 \pm 144$	$20 \pm 161$	$0 \pm 142$	$0 \pm 134$
Pressure (Gbar)*	$90.4 \pm 13.1$	$119.7 \pm 21.8$	$164.6 \pm 27.3$	$123.3 \pm 21.4$	$140.4 \pm 29.2$	$140.7 \pm 33.4$
Energy delivered to fuel (kJ)*	$8.3 \pm 0.8$	$10.1 \pm 1.6$	$12.2 \pm 1.6$	$11.2 \pm 1.6$	$11.1 \pm 1.6$	$11.6 \pm 2.1$
Compression yield (kJ)*	$5.2 \pm 0.2$	$6.3 \pm 0.3$	$7.8 \pm 0.4$	$9.9 \pm 0.5$	$9.1 \pm 0.4$	$6.0 \pm 0.2$
Self-heating yield (kJ)*	$2.6 \pm 0.2$	$3.5 \pm 0.4$	$6.1 \pm 0.5$	$6.9 \pm 0.7$	$7.9 \pm 0.6$	$3.1 \pm 0.3$

thick capsule driven at 350 TW still has sufficient mass remaining to maintain good compression and has not yet burned through to the fuel.

Three shots,  $N130812$ ,  $N131219$ , and  $N140707$ , representing the three different ablator thicknesses, were shot at nominally the same laser peak power of  $354 \pm 5$  TW. It can be seen that a higher DT yield, with comparable DSR, and higher inferred hot spot pressure were achieved with the progressively thinner capsules. This can be attributed to the gain in velocity ( $v$ ) due to the thinner ablator. [ $v \sim \sqrt{(2E/m)}$ , where  $E$  is absorbed energy and  $m$  is ablator mass. The reduced  $m$  yields higher  $v$  for the same absorbed energy. Since pressure ( $P$ )  $\sim v^3$  and fusion yield ( $Y_n$ )  $\sim P^2$ , then  $Y_n \sim v^6$  [23].] Another case study, comparing  $N140311$  ( $T-1$ ) to  $N131119$  ( $T0$ ), shows that identical primary neutron yields were achieved, but in the case of the 10% thinner ablator, at 34 TW less power and 160 kJ less energy. Furthermore, both x-ray and neutron imaging of  $N140311$  (see Fig. 2) and  $N131119$  (see Ref. [5]) show very similar shapes, indicating that the relative performance improvement of  $N140311$  is due to the increased velocity.

Two  $T-1$  DT shots,  $N131219$  and  $N140225$ , were shot at near-identical configurations to test the repeatability of the thin shell implosions.  $N140225$  incorporated a trough cone fraction change from 45% to 38% (where the trough is defined as the period in the pulse between 2.5 and 8.5 ns, and cone fraction as the inner beams power over the total

laser power), and overall laser energy was 4% low. There were also small differences in the smoothness and low-mode shape of the DT ice layer grown in both cases ( $N140225$  had a single ice groove of  $1600 \mu\text{m}^2$ ,  $N131219$  had none). Nonetheless, the integrated performance of the two shots is in very close agreement, with primary neutron

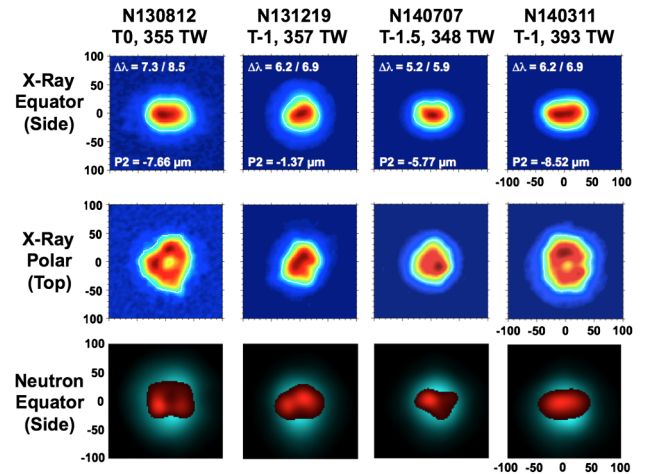


FIG. 2 (color online). Time-integrated x-ray self-emission images from the equator and the pole, and the superposition of primary (13–17 MeV, red) and downscattered (6–12 MeV, cyan) neutron images for  $N130812$ ,  $N131219$ ,  $N140707$ , and  $N140311$ . Wavelength separations ( $\Delta\lambda$ ) are denoted as  $\lambda_{30}/\lambda_{23}$  (in Å).

yields within 7%, demonstrating the stability of the implosions. This also indicates that we may be in a regime where we are relatively insensitive to defects and/or small-scale surface roughness of the ice.

Images of the imploded DT hot spot show that thinner ablators provide better shape control. Figure 2 displays the time-integrated x-ray self-emission at  $> 6$  keV energies as viewed from the equatorial and polar lines of sight. The three-color wavelength separations ( $\Delta\lambda$ ) were decreased for the successively thinner ablators at the  $354 \pm 5$  TW laser level. Less  $\Delta\lambda$  was necessary to maintain the same (or better) symmetry at a given power for the thinner ablators. This allows for more flexibility to compensate for hot spot distortions using cross beam transfer.

As the laser power and energy were increased, the hot spot trend toward oblateness was observed to be similar in the thinner shell capsules as what was seen with the nominal thickness, primarily due to deficiencies in inner beam propagation to the waist of the hohlraum (images for *N131219* versus *N140311* compare the thin shells imploded with 1.62 MJ, 357 TW versus 1.75 MJ, 393 TW). Also shown in Fig. 2 are the primary (13–17 MeV) and downscattered (6–12 MeV) neutron images overlaid, which provide the shape of the neutron-producing core and cold fuel, respectively [24,25]. For all shots discussed here, the primary neutron image  $P_0$  agrees to within 10% of the x-ray image  $P_0$ . As the x-ray image is integrated over the x-ray emission time and the neutron image integrates over the nuclear burn duration, a similar shape indicates that the neutron-producing region is analogous to the hot x-ray emitting region. Differences may indicate more complex 3D shapes captured by the different lines of sights of the detectors. It is obvious that although a combination of thinner shells,  $\Delta\lambda$  adjustments, and power limitations can improve shape, controlling the low-mode hot spot shape remains a challenge.

Implosions fielded on a higher adiabat have shown to be more robust to mix [6], presumably because of a larger ablative stabilization effect and reduced convergence. Detailed growth factor measurements based on the amplification in optical depth of applied perturbations have shown a  $5\times$  reduction in growth at the dominant mode 60 (the peak mode) for the high foot as compared to the low foot [26–28]. The enhanced stability can also be understood by comparing the IFAR of these respective implosions as the capsule converges to smaller radii, as shown in Fig. 3. The predicted IFAR is shown for a nominal  $T0$  and thinner  $T-1$  shell driven with the same high-foot pulse, compared against a representative well-performing low-foot drive. Other than a small region around  $R_{in} = 600 \mu\text{m}$ , both high-foot driven ablators show lower and therefore more stable IFARs than the low-foot nominal thickness capsule.

Despite the higher IFAR, measurements of the mix mass [30] for these thinner capsules still show very low levels ( $< 200$  ng) of mix. The thinner shell should be more

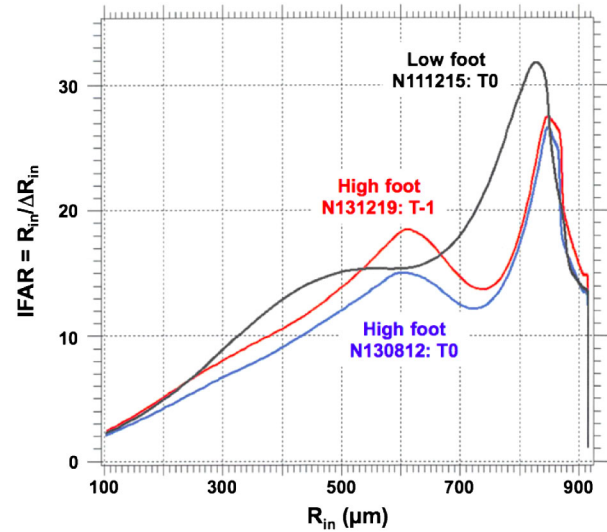


FIG. 3 (color online). 2D ARES [29] calculations show that the high-foot IFAR is  $\sim 60\%$  of the low foot at the steepest region where most of the ablation-front instability growth occurs. For most of the implosion, the  $T-1$  shell high-foot IFAR is below that of the low-foot  $T0$ .

susceptible to ablation front feedthrough as well as shell breakup. Furthermore, the amount of ablator mass shielding the inner ablator is reduced, potentially exposing the region to increased preheat. This would raise the Atwood number and cause mixing at the fuel-ablator interface to increase. Figure 4 shows the DT neutron yield as a function of x-ray enhancement ratio for the full set of cryogenic DT

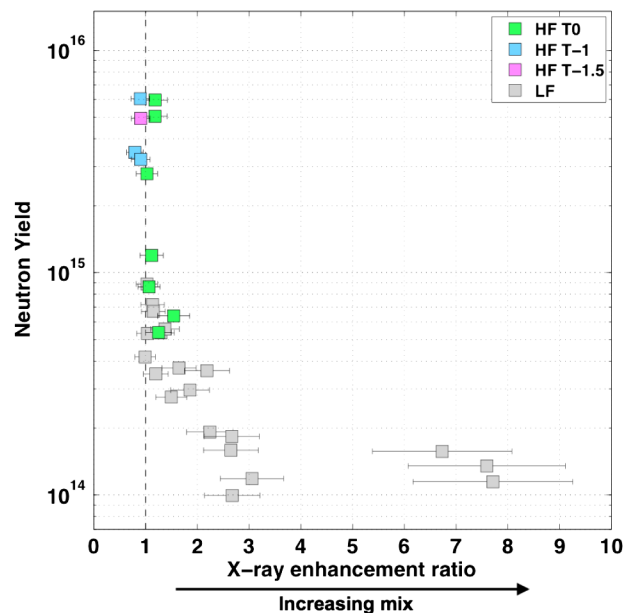


FIG. 4 (color online). DT neutron yield versus x-ray enhancement ratio for the cryogenic DT implosions completed on the NIF. "HF" refers to high-foot implosions; "LF" refers to low-foot implosions. The thinner shell implosions continue to cluster around the zero mix region.

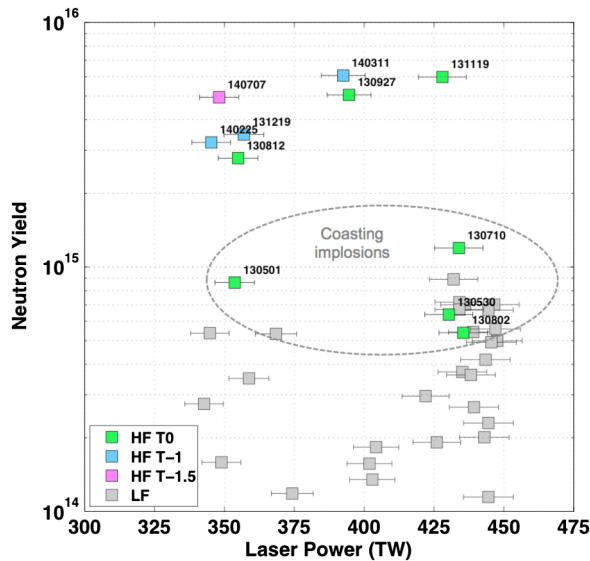


FIG. 5 (color online). DT neutron yield versus peak laser power. The improvement in yield with thinner ablators at comparable laser powers can be seen at 350 and 390 TW. The three  $T-1$  shell capsules follow a similar scaling with laser power as the  $T_0$ .

implosions with CH shells completed on the NIF. The  $T-1$  and  $T-1.5$  thin shell implosions continue to cluster with the  $T_0$  high-foot implosions, with no strong evidence of ablator significantly mixing into the hot spot. This is consistent with the good neutron performance and high  $T_{\text{ion}}$  mentioned earlier, as a high- $Z$  mix would radiatively cool the hot spot and quench the burn.

A plot of the total neutron yield versus laser peak power (Fig. 5) shows the absolute performance of these thin shell capsules as compared to implosions with the nominal thickness capsule. The colored points were driven with a high-adiabat three-shock, no-coast pulse shape (where “no coast” designates an extended laser pulse leaving  $< 1$  ns between the end of the pulse and capsule peak compression). As the backscatter fraction did not change much as a function of capsule thickness, it can be assumed that the absorbed peak power scales with incident peak power. It can be seen that the yield performance for the series of three  $T_0$  capsules monotonically increases with increasing laser power, and the three  $T-1$  capsules follow a similar slope. Shots taken at the same laser power show the improved performance of the thinner shells over the  $T_0$  capsule. While shape plays a role in the improved performance, it is the increased velocity that dominates the scaling to increased fusion yield ( $Y_n \sim v^6$ , as described above). The inferred peak implosion fuel velocities, derived from the 2DConA-measured velocities with corrections applied for delivered laser, capsule metrology, fuel mass, and measured stagnation (bang) time [31,32] as listed in Table I, scale as the square root of laser power. The highest fuel velocities achieved with CH ablators, exceeding

370 km/s, have been demonstrated with these thinner ablators.

Of particular interest are the implosion energetics for each shot. Table I shows the inferred energy delivered to the fuel, as well as the components of yield derived from compression and  $\alpha$ -particle self-heating. The methodology for determining these quantities is given in Ref. [5]. With the exception of  $N140225$  and  $N131219$ , the sum of the compression and self-heating yields of the thinner capsules exceeds the energy delivered to the fuel (outside of error bars), with a significant fraction of the overall yield due to  $\alpha$ -particle generation and deposition within the fuel—a crucial criterion for hot spot assembly and confinement. Shot  $N140311$  exhibited nearly equal parts self-heating and compression yield, demonstrating that we are approaching the bootstrapping regime, where the  $\alpha$ -particle deposition will result in further burn and exponential gains in yield.

The improvement in hot spot symmetry and increased implosion speed concomitant with the thinner ablators is in good agreement with the predictions from 2D HYDRA [33] integrated hohlraum-capsule simulations. Postshot modeling indicates that time-dependent symmetry swings are having a significant (at least  $5\times$ ) impact on the neutron yield, and understanding and reducing these symmetry swings is a current topic of investigation [34].

In summary, high-foot implosions using 10% and 15% thinner ablators have been conducted at the National Ignition Facility. These implosions have achieved velocities of over 370 km/s with little to no indications of mix—a considerable achievement over the NIC implosions which measured mix masses of up to 3000–4000 ng at fuel velocities between 300 and 340 km/s [4]. Future work will explore driving the implosions to yet higher velocities by a combination of increased laser power and further reductions in ablator thickness. The challenge will continue to be balancing the shape control with the higher velocity, while maintaining a stable implosion. Plans also include exploring alternate hohlraum geometries to control the in-flight and hot spot shape, different hohlraum materials [35], and adiabat shaping using laser pulse modifications to reduce the adiabat [36,37].

We wish to thank the NIF operations team. This work was performed under the auspices of the U.S. Department of Energy by Lawrence Livermore National Laboratory under Contract No. DE-AC52-07NA27344.

- 
- [1] J. D. Lindl, P. Amendt, R. L. Berger, S. G. Glendinning, S. H. Glenzer, S. W. Haan, R. L. Kauffman, O. L. Landen, and L. J. Suter, *Phys. Plasmas* **11**, 339 (2004).
  - [2] G. H. Miller, E. I. Moses, and C. R. Wuest, *Nucl. Fusion* **44**, S228 (2004).
  - [3] E. I. Moses, R. N. Boyd, B. A. Remington, C. J. Keane, and R. Al-Ayat, *Phys. Plasmas* **16**, 041006 (2009).

- [4] M. J. Edwards, P. K. Patel, J. D. Lindl, L. J. Atherton, S. H. Glenzer, S. W. Haan, J. D. Kilkenny, O. L. Landen, E. I. Moses, A. Nikroo *et al.*, *Phys. Plasmas* **20**, 070501 (2013).
- [5] O. A. Hurricane, D. A. Callahan, D. T. Casey, P. M. Celliers, C. Cerjan, E. L. Dewald, T. R. Dittrich, T. Doppner, D. E. Hinkel, L. F. B. Hopkins *et al.*, *Nature (London)* **506**, 343 (2014).
- [6] H. S. Park, O. A. Hurricane, D. A. Callahan, D. T. Casey, E. L. Dewald, T. R. Dittrich, T. Doppner, D. E. Hinkel, L. F. Berzak Hopkins, S. Le Pape *et al.*, *Phys. Rev. Lett.* **112**, 055001 (2014).
- [7] T. R. Dittrich, O. A. Hurricane, D. A. Callahan, E. L. Dewald, T. Doppner, D. E. Hinkel, L. F. Berzak Hopkins, S. Le Pape, T. Ma, J. L. Milovich, J. C. Moreno, P. K. Patel, H.-S. Park, B. A. Remington, J. D. Salmonson, and J. L. Kline, *Phys. Rev. Lett.* **112**, 055002 (2014).
- [8] D. G. Hicks, N. B. Meezan, E. L. Dewald, A. J. Mackinnon, R. E. Olson, D. A. Callahan, T. Doppner, L. R. Benedetti, D. K. Bradley, P. M. Celliers *et al.*, *Phys. Plasmas* **19**, 122702 (2012).
- [9] D. G. Hicks, B. K. Spears, D. G. Braun, R. E. Olson, C. M. Sorce, P. M. Celliers, G. W. Collins, and O. L. Landen, *Phys. Plasmas* **17**, 102703 (2010).
- [10] N. B. Meezan, A. J. Mackinnon, D. G. Hicks, E. L. Dewald, R. Tommasini, S. Le Pape, T. Doppner, T. Ma, D. R. Farley, D. H. Kalantar *et al.*, *Phys. Plasmas* **20**, 056311 (2013).
- [11] D. T. Casey, V. A. Smalyuk, R. E. Tipton, J. E. Pino, G. P. Grim, B. A. Remington, D. P. Rowley, S. V. Weber, M. Barrios, L. R. Benedetti *et al.*, *Phys. Plasmas* **21**, 092705 (2014).
- [12] R. Tommasini (to be published).
- [13] S. W. Haan, J. D. Lindl, D. A. Callahan, D. S. Clark, J. D. Salmonson, B. A. Hammel, L. J. Atherton, R. C. Cook, M. J. Edwards, S. Glenzer *et al.*, *Phys. Plasmas* **18**, 051001 (2011).
- [14] O. A. Hurricane, D. A. Callahan, D. T. Casey, E. L. Dewald, T. R. Dittrich, T. Doppner, M. A. Barrios Garcia, D. E. Hinkel, L. F. Berzak Hopkins, P. Kervin *et al.*, *Phys. Plasmas* **21**, 056314 (2014).
- [15] J. R. Rygg, O. S. Jones, J. E. Field, M. A. Barrios, L. R. Benedetti, G. W. Collins, D. C. Eder, M. J. Edwards, J. L. Kline, J. J. Kroll *et al.*, *Phys. Rev. Lett.* **112**, 195001 (2014).
- [16] P. Michel, S. H. Glenzer, L. Divol, D. K. Bradley, D. Callahan, S. Dixit, S. Glenn, D. Hinkel, R. K. Kirkwood, J. L. Kline *et al.*, *Phys. Plasmas* **17**, 056305 (2010).
- [17] V. Y. Glebov, D. D. Meyerhofer, T. C. Sangster, C. Stoeckl, S. Roberts, C. A. Barrera, J. R. Celeste, C. J. Cerjan, L. S. Dauffy, D. C. Eder *et al.*, *Rev. Sci. Instrum.* **77**, 10E715 (2006).
- [18] D. L. Bleuel, C. B. Yeaman, L. A. Bernstein, R. M. Bionta, J. A. Caggiano, D. T. Casey, G. W. Cooper, O. B. Drury, J. A. Frenje, C. A. Hagmann *et al.*, *Rev. Sci. Instrum.* **83**, 10D313 (2012).
- [19] M. Gatu Johnson, J. A. Frenje, D. T. Casey, C. K. Li, F. H. Seguin, R. Petrasso, R. Ashbranner, R. M. Bionta, D. L. Bleuel, E. J. Bond *et al.*, *Rev. Sci. Instrum.* **83**, 10D308 (2012).
- [20] A reanalysis of the neutron time of flight detector data due to a recently discovered nonlinear detector response at high neutron yields has resulted in updated  $T_{\text{ion}}$  and DSR values as compared to Ref. [5].
- [21] J. A. Frenje, R. Bionta, E. J. Bond, J. A. Caggiano, D. T. Casey, C. Cerjan, J. Edwards, M. Eckart, D. N. Fittinghoff, S. Friedrich *et al.*, *Nucl. Fusion* **53**, 043014 (2013).
- [22] A. Mackinnon, J. Kline, S. Dixit, S. Glenzer, M. Edwards, D. Callahan, N. Meezan, S. Haan, J. Kilkenny, T. Doppner *et al.*, *Phys. Rev. Lett.* **108**, 215005 (2012).
- [23] R. Betti, P. Y. Chang, B. K. Spears, K. S. Anderson, J. Edwards, M. Fatenejad, J. D. Lindl, R. L. McCrory, R. Nora, and D. Shvarts, *Phys. Plasmas* **17**, 058102 (2010).
- [24] F. E. Merrill, D. Bower, R. Buckles, D. D. Clark, C. R. Danly, O. B. Drury, J. M. Dzenitis, V. E. Fatherley, D. N. Fittinghoff, R. Gallegos *et al.*, *Rev. Sci. Instrum.* **83**, 10D317 (2012).
- [25] P. Volegov, C. R. Danly, D. N. Fittinghoff, G. P. Grim, N. Guler, N. Izumi, T. Ma, F. E. Merrill, A. L. Warrick, C. H. Wilde *et al.*, *Rev. Sci. Instrum.* **85**, 023508 (2014).
- [26] V. A. Smalyuk, D. T. Casey, D. S. Clark, M. J. Edwards, S. W. Haan, A. Hamza, D. E. Hoover, W. W. Hsing, O. Hurricane, J. D. Kilkenny *et al.*, *Phys. Rev. Lett.* **112**, 185003 (2014).
- [27] D. T. Casey, V. A. Smalyuk, K. S. Raman, J. L. Peterson, L. Berzak Hopkins, D. A. Callahan, D. S. Clark, E. L. Dewald, T. R. Dittrich, S. W. Haan *et al.*, *Phys. Rev. E* **90**, 011102 (2014).
- [28] K. S. Raman, V. A. Smalyuk, D. T. Casey, S. W. Haan, D. E. Hoover, O. A. Hurricane, J. J. Kroll, A. Nikroo, J. L. Peterson, B. A. Remington *et al.*, *Phys. Plasmas* **21**, 072710 (2014).
- [29] R. M. Darlington, T. L. McAbee, and G. Rodrigue, *Comput. Phys. Commun.* **135**, 58 (2001).
- [30] T. Ma, P. K. Patel, N. Izumi, P. T. Springer, M. H. Key, L. J. Atherton, L. R. Benedetti, D. K. Bradley, D. A. Callahan, P. M. Celliers *et al.*, *Phys. Rev. Lett.* **111**, 085004 (2013).
- [31] D. A. Callahan, N. B. Meezan, S. H. Glenzer, A. J. Mackinnon, L. R. Benedetti, D. K. Bradley, J. R. Celeste, P. M. Celliers, S. N. Dixit, and T. Doppner, *Phys. Plasmas* **19**, 056305 (2012).
- [32] O. L. Landen, J. Edwards, S. W. Haan, H. F. Robey, J. Milovich, B. K. Spears, S. V. Weber, D. S. Clark, J. D. Lindl, B. J. Macgowan *et al.*, *Phys. Plasmas* **18**, 051002 (2011).
- [33] M. M. Marinak, G. D. Kerbel, N. A. Gentile, O. Jones, D. Munro, S. Pollaine, T. R. Dittrich, and S. W. Haan, *Phys. Plasmas* **8**, 2275 (2001).
- [34] A. Kritcher and D. E. Hinkel (private communication).
- [35] T. Doppner (to be published).
- [36] V. N. Goncharov, J. P. Knauer, P. W. McKenty, P. B. Radha, T. C. Sangster, S. Skupsky, R. Betti, R. L. McCrory, and D. D. Meyerhofer, *Phys. Plasmas* **10**, 1906 (2003).
- [37] K. Baker (to be published).